

Innovative and industrially viable approach to fabricate AlOx rear passivated ultra-thin Cu(In, Ga)Se₂ (CIGS) solar cells

Peer-reviewed author version

BIRANT, Gizem; DE WILD, Jessica; KOHL, Thierry; BULDU KOHL, Dilara; BRAMMERTZ, Guy; MEURIS, Marc; POORTMANS, Jef & VERMANG, Bart (2020) Innovative and industrially viable approach to fabricate AlOx rear passivated ultra-thin Cu(In, Ga)Se₂ (CIGS) solar cells. In: Solar energy (Print), 207 , p. 1002 -1008.

DOI: 10.1016/j.solener.2020.07.038

Handle: <http://hdl.handle.net/1942/31684>

Innovative and industrially viable approach to fabricate AlO_x rear passivated ultra-thin Cu(In, Ga)Se₂ (CIGS) solar cells.

Gizem Birant^{1,2,3,a}, J. de Wild^{1,2,3}, T. Kohl^{1,2,3}, D.G. Buldu^{1,2,3}, G. Brammertz^{1,2,3}, M. Meuris^{1,2,3}, J. Poortmans^{1,3,4,5}, B. Vermang^{1,2,3}

¹ Institute for Material Research (IMO), Hasselt University (partner in Solliance), Agoralaan gebouw H, Diepenbeek, 3590, Belgium

² Imec division IMOMECEC (partner in Solliance), Wetenschapspark 1, 3590 Diepenbeek, Belgium.

³ EnergyVille, Thorpark, Poort Genk 8310 & 8320, 3600, Belgium

⁴ imec (partner in Solliance), Kapeldreef 75, Leuven, 3001, Belgium

⁵ Department of Electrical Engineering, KU Leuven, Kasteelpark Arenberg 10, 3001 Heverlee, Belgium

^a gizem.birant@imec.be

Abstract

In this work, an industrially viable and novel rear surface passivation approach for Copper Indium Gallium di-Selenide, Cu(In, Ga)Se₂, CIGS, ultra-thin (500nm) solar cells is developed. The passivation layer was deposited by atomic layer deposition (ALD), and an alkali treatment was applied via spin coating. It was observed that selenization of the samples is required to create contact openings. The openings were visualized by SEM, and these results were supported by EDS. The impact of the oxide layer's thickness, as well as the alkali solution's molarity, was studied. Solar cells were produced for the optimal combination of these two parameters. As a result, with a relative 13% increase, the highest V_{oc} of 623mV was achieved. Hence, the efficiency of the passivated solar cell was relatively increased by one-third, by using an industrially feasible, fast, and repeatable technique.

1. Introduction

Today, one of the most efficient thin-film photovoltaic (PV) technology is CIGS multi-crystalline thin-film solar cells (Green et al., 2020). In order to compete with other solar cell technologies, the production costs should be reduced, and the structure should be simplified. To make cheaper solar cells, reducing the thickness of the absorber layer is one solution. However, reducing the thickness of the absorber layer has drawbacks like incomplete absorption and increased back-contact recombination, both resulting in power conversion efficiency losses (Naghavi et al., 2016), (Umehara et al., 2016). One solution is to implement a rear surface passivation layer, which has the potential to reduce rear surface recombination velocity and increase rear internal reflection (Poncelet et al., 2018). However, CIGS solar cells generally benefit from the sodium (Na) coming from the soda-lime glass substrate (Li et al., 2019), (Rudmann, 2004). Usage of a dielectric layer at the rear surface, such as alumina (Al₂O₃) which is an ideal passivation layer (Groner et al., 2002), (Poncelet et al., 2017), unfortunately, acts as an electron and diffusion barrier layer, and thus prevents current flow and the Na diffusion. In order to overcome these problems, there needs to be contact openings in this passivation layer. In reference (Vermang et al., 2014b), the rear surface passivation technique used for silicon (Si) solar cells was implemented to CIGS solar cells. In that study, Al₂O₃ was

46 used as the rear surface passivation layer, and nano-sized point contact openings were realized
 47 via chemical bath deposited CdS nanoparticles (Vermang et al., 2014b). Over the years, many
 48 research groups developed and applied different techniques to generate these openings in
 49 various dielectric layers, see (Birant et al., 2019). Almost all of the proven methods – e.g.,
 50 using nanoparticles, e-beam or nano-imprint lithography – are well controlled, but also
 51 expensive, time-consuming or not applicable for larger areas, see (Necas and Klapetek, 2012),
 52 (Vermang et al., 2015) and (Yin et al., 2017).

53 D. Ledinek et al. previously proposed using a very thin layer of Al₂O₃ as rear surface
 54 passivation in combination with NaF evaporation to enhance the electrical characteristics of
 55 CIGS solar cells. In their study, the surface passivation layer is claimed to have a porous
 56 structure that allows direct contact between Mo and CIGS, and they supported their claims with
 57 TEM and XPS analysis (Ledinek et al., 2018). The proposed method in our study is to spin-
 58 coat the NaF on top of the Al₂O₃ passivation layer, which will generate contact openings during
 59 selenization. The generated contact openings were visualized by SEM prior to and after CIGS
 60 deposition. The aim is to prove that by using a simple, cost-effective, and fast process, it is
 61 possible to passivate the rear surface of ultra-thin CIGS solar cells, and hence, increase the
 62 efficiency, i.e., make it cheaper and industrially feasible.

63

64 2. Experimental details:

65

66 In this section, the implementation of the novel rear surface passivation approach into the
 67 standard solar cell structure is explained. The proposed method is to spin-coat sodium fluoride
 68 (NaF) on top of the Al₂O₃ passivation layer to generate the contact openings during
 69 selenization. Al₂O₃ passivation layer was deposited through atomic layer deposition (ALD) at
 70 300°C. During the depositions, trimethylaluminum (TMA) was used as the precursor, and H₂O
 71 used as the reactant. The nm/cycle rate was calculated to be 0.17, by measuring the Al₂O₃
 72 thickness on Mo with ellipsometry and assuming a constant growth rate with time. The
 73 proposed rear surface passivation approach is integrated into the standard stack:
 74 SLG/Mo/AlO_x/CIGS/CdS/i-ZnO/ZnO:Al/Ni-Ag-Ni grids, where solar cell devices have
 75 ultrathin (500 nm), single-stage and ungraded, i.e. without Ga-grading, CIGS absorber layers
 76 with ([Cu]/([Ga] + [In]) = 0.83 and ([Ga]/([Ga] + [In]) = 0.33, with active area of 0.5cm². In
 77 this study, a flat Ga profile was preferred to eliminate reciprocal rear surface passivation effects
 78 of Ga-grading (Vermang et al., 2014b), (de Wild et al., 2019).

79

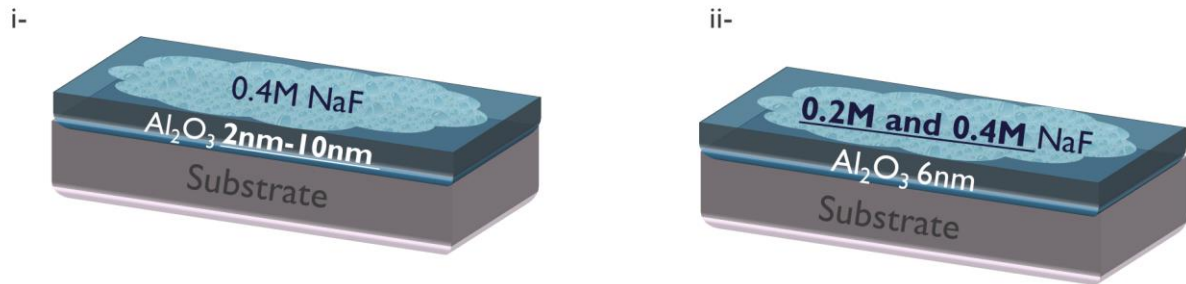
80 **Table-1** Overview of all steps required to produce sample Set 1 and Set 2

81

Step	Sample Set 1	Sample Set 2
1	Substrate cleaning	Substrate cleaning
2	<i>Al₂O₃ passivation layer deposition (2nm-10nm)</i>	Al ₂ O ₃ passivation layer deposition (6nm)
3	NaF spin coating (0.4M)	<i>NaF spin coating (0.2M-0.4M)</i>
4	Selenization	Selenization

82

83 In order to identify the optimal parameters, two sets of samples were prepared: altering, first,
84 the thickness of the dielectric layer (Set 1), and second the molarity of the alkali solution (Set
85 2); see Table-1 and Figure-1. For both sets, and for each parameter, two different samples were
86 produced: one for characterization and one for solar cell production. As the substrate, 3mm
87 thick soda-lime glass (SLG) with Si(O, N) barrier layer, which has 300nm molybdenum (Mo)
88 as the rear contact, was used.



89 **Figure 1** Sketch of the two sets of samples with altering i- Al₂O₃ thickness and ii- NaF
90 molarity; to investigate their effects on passivation characteristics and openings.
91

92
93 For Set 1, five different Al₂O₃ layer thicknesses were tested, starting from 2nm and ending with
94 10nm, by 2nm steps. Following the Al₂O₃ depositions, 0.4M NaF was spin-coated on those
95 layers. Characterization samples were selenized at 540°C, for 10 minutes, in order to mimic
96 the absorber layer deposition environment. For selenization, a quad-elliptical radiant heating
97 chamber and pure selenium particles were used. This process has occurred under a vacuum. To
98 monitor the formation of the openings, characterization samples underwent several
99 characterization steps. As a first step, scanning electron microscopy (SEM) imaging and
100 energy-dispersive X-ray spectroscopy (EDS) analysis was done with a Tescan and Bruker
101 SEM. In order to calculate the density of the opening-like structures, a data analysis software
102 named Gwyddion was used. This software can analyze and compare the height difference
103 between the two layers by using SEM images (Necas and Klapek, 2012). In our case, it spots
104 the height difference between the alumina layer and the molybdenum back contact and gives
105 the percentage of the contact openings. An example of the Gwyddion analysis is shown in
106 Figure-2-a. We used three different SEM pictures with varying magnifications for each sample,
107 and use the arithmetic average of those three images while calculating the surface coverage
108 (SC) ratios.

109 In order to decide the optimal thickness of the dielectric layer, samples that were completed as
110 solar cells were used. According to the IV results, the optimal thickness was chosen as 6nm.
111 Concerning the molarity of the NaF solution, i.e., Set 2, two different molarities were tested,
112 0.2M and 0.4M, with a 6nm Al₂O₃ layer. Also, regarding the necessity of this treatment,
113 samples without any alkali treatment, i.e., 0 M condition, were prepared. Similar to Set 1, these
114 samples also underwent the same characterization steps, and 0.4M was chosen as the optimal
115 molarity for our approach. Exact reasons why we chose the thickness and the molarity as 6 nm
116 and 0.4M, respectively, will be shared in the following section.

117 Production steps of the reference and passivated solar cells are shared in Table-2. For the
118 passivated solar cell, the aforementioned optimal parameters were used, and the detailed
119 explanation of the steps for the reference sample can be found in (de Wild et al., 2019).

120 The completed solar cells were characterized by JV measurement under AM 1.5 illumination.
 121 The Voc, Jsc, FF, and efficiency were derived from the JV curves. Twelve cells were measured
 122 for reference and passivated samples, and the arithmetic average results are shared in Table-3.
 123 The values for saturated current density (J_0), shunt and series resistances (R_{sh} and R_s) are
 124 calculated from the dark JV measurement using a MATLAB routine. J_0 values are extracted
 125 from the JV curve, which is corrected for R_s and R_{sh} , with a 1-diode model.

126
 127 **Table-2** Overview of all steps required to produce reference Cu(In, Ga)Se₂ solar cells and
 128 Al₂O₃ rear surface passivated cells with contacts.

Step	Description	
	<u>Reference</u>	<u>Passivated</u>
1	Substrate cleaning	Substrate cleaning
2		<i>Al₂O₃ passivation layer deposition</i>
3	NaF spin coating	NaF spin coating
4	1 stage ultra-thin (500 nm) CIGS absorber co-evaporation	1 stage ultra-thin (500 nm) CIGS absorber co-evaporation
5	CBD CdS buffer deposition	CBD CdS buffer deposition
6	i-ZnO and ZnO:Al window sputtering	i-ZnO and ZnO:Al window sputtering
7	Ni/Al/Ni front contact evaporation	Ni/Al/Ni front contact evaporation

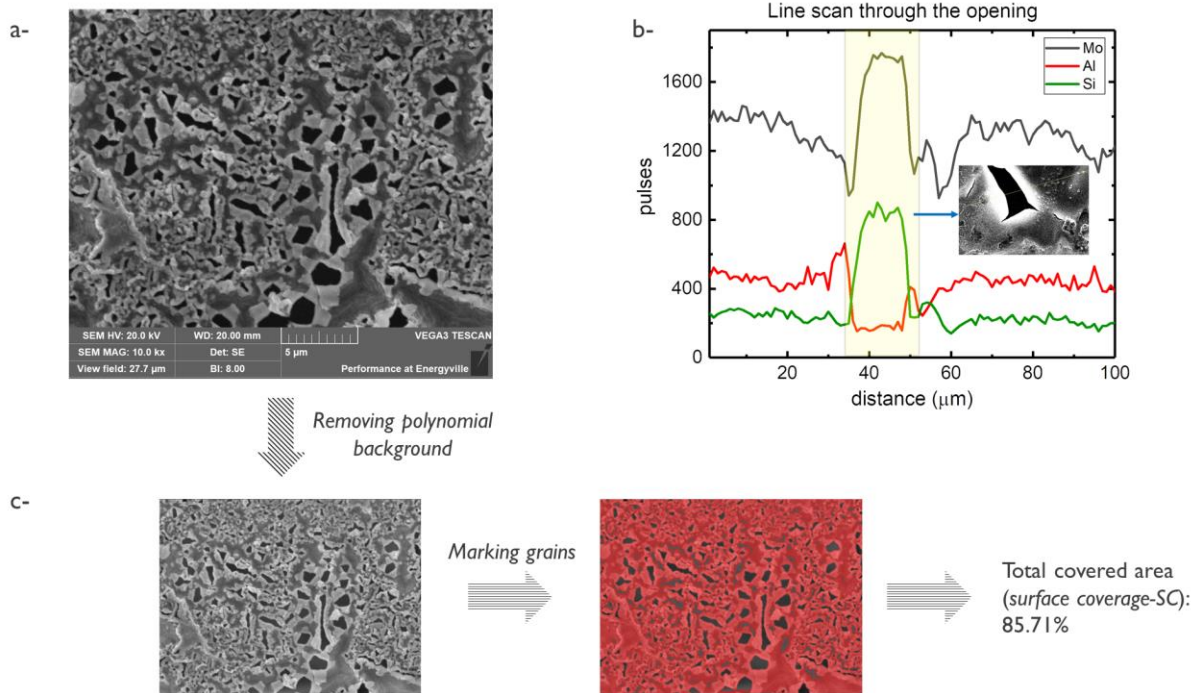
130
 131 EQE was measured under dark conditions and scanned through the wavelength interval of 350-
 132 1300nm in 5nm steps. For the passivated sample, Jsc values were extracted from the EQE, and
 133 the efficiencies recalculated accordingly. PL and TRPL measurements were carried out in a
 134 photo spectrometer from Picoquant with a TimeHarp 260 single-photon counter for the time-
 135 resolved measurements. The excitation intensity is approximately 0.2 W cm⁻², the repetition
 136 rate is 3 MHz, and the wavelength is 532nm.

137 138 **3. Results and discussion:**

139 140 **3.1 Creation of the contact openings:**

141 In order to interpret the effect of NaF spin-coating on the alumina passivation layer during
 142 selenization, two characterization sample sets were used as described above. To monitor the
 143 results of this process, SEM imaging was done before and after this step, and results were
 144 supported with EDS analysis, see Figure-2-b. In the end, it was experimentally proven that,
 145 during the selenization, in certain cases, contact openings are formed in the passivation layer.
 146 The impact of the thickness of the dielectric layer and the molarity of the alkali solution on the
 147 density and size of the contact openings was also investigated, see Figure-3-a. By considering
 148 the change in the surface coverage ratios as well as the shape and the size of the openings,
 149 samples that were finished as solar cells were used to assess the impact of this difference on
 150 open-circuit voltage, Voc.

151



152
153

154 **Figure 2** a-SEM picture of the optimal sample after selenization and b- EDS line scan to prove
155 the existence of the openings in the dielectric layer (inset SEM picture of the analyzed sample)
156 and c- example of Gwyddion analysis with calculated surface coverage ratio.

157

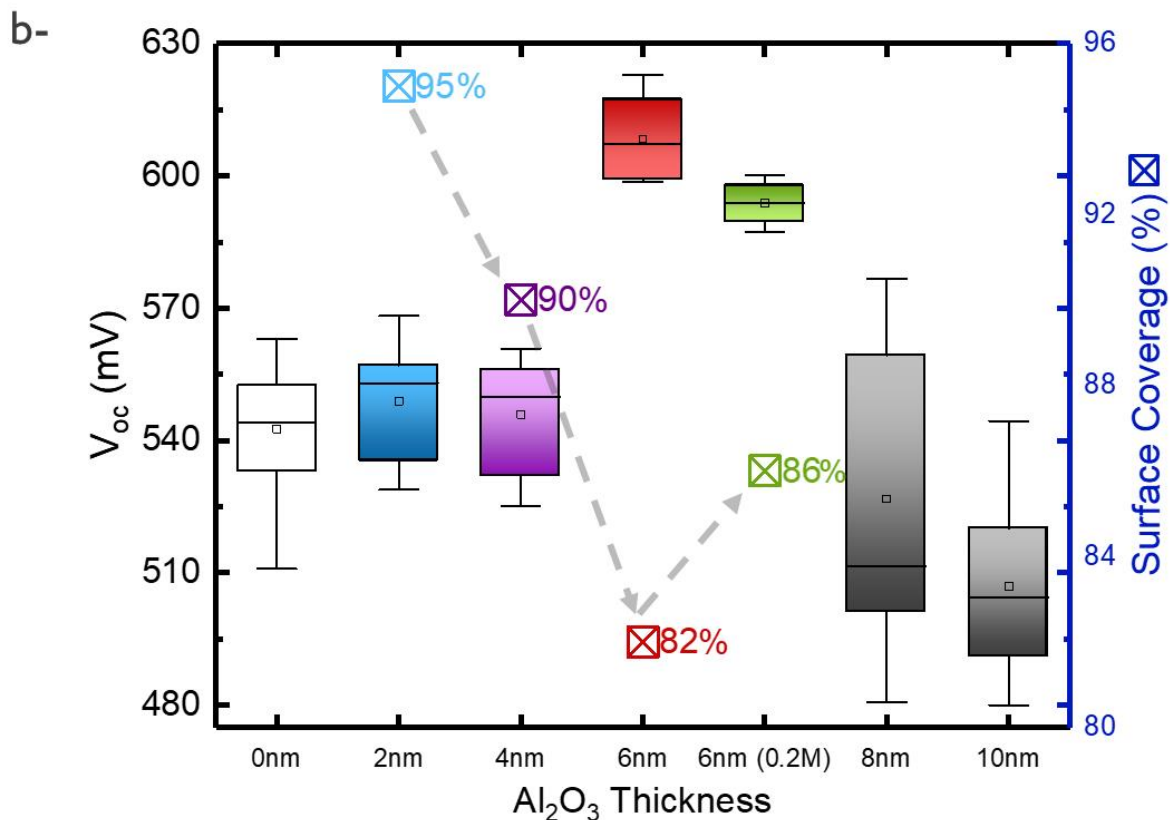
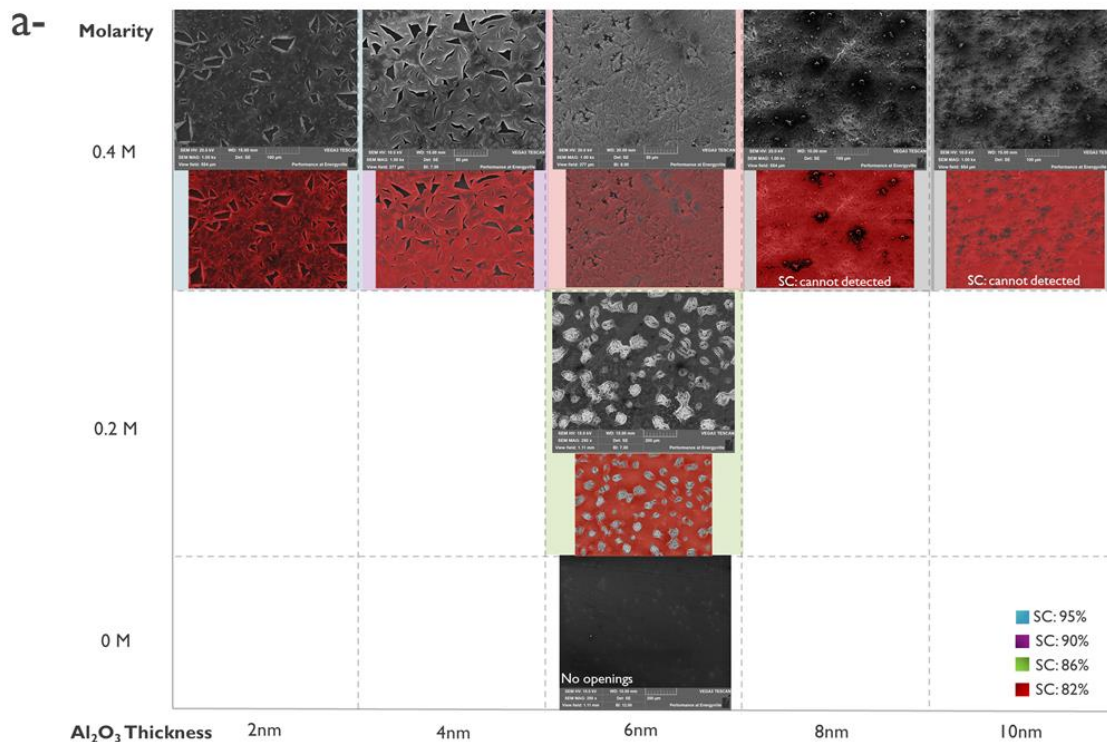
158 As can be seen from Fig.3-b, there is an inverse relation between Voc and the SC. The
159 discussion part for this graph is divided into two subsections: 3.1.1- effect of the thickness of
160 the Al₂O₃ layer and 3.1.2- effect of the molarity of the alkali solution. In the end, there is
161 section iii, which will contain the discussion associated with the solar cells prepared with the
162 optimal conditions decided according to subsections 3.1-a and 3.1-b.

163

164 3.1.1 Effect of the thickness of the alumina layer, Set 1:

165 For this set, in order to monitor the effect of the thickness of the Al₂O₃ layer, we kept the
166 molarity of the alkali solution as 0.4M for all of the samples. As can be seen from Fig.3-a, for
167 8nm and 10nm thick alumina layers, we could not detect any opening like structure. On the
168 other hand, for 2nm, 4nm, and 6nm thick alumina layers, we were able to observe openings in
169 the alumina layer. For those samples, the surface coverage ratios were calculated with the help
170 of Gwyddion software, as described in Fig.2-c. If Fig.3.b is investigated further in terms of
171 the thickness of the Al₂O₃ layer, it can be seen that until the 8nm thick dielectric layer, the Voc is
172 improved compared to the reference. However, for 8nm and 10nm thick Al₂O₃ layer, the Voc
173 is worse than the rest of the Set-1, including the reference. This information is vital for us to
174 understand that, with our novel contacting approach, thicknesses over 6nm is not suitable for
175 rear surface passivation.

176



177
 178 **Figure 3** a-Molarity vs. thickness of the aluminum oxide layer with insets of SEM images,
 179 Gwyddion masks and surface coverage ratios of samples belongs to Set 1 and Set 2, and b-
 180 Open circuit voltage and surface coverage ratios vs. thickness of the aluminum oxide layer for
 181 the same set of samples; box charts represents the V_{oc} and boxes represents the SC (%). The
 182 arrows are given to emphasize the inverse relation between V_{oc} and SC in terms of Al₂O₃ thickness.

183 When we compare our surface coverage (SC) results with other groups, we realized a slight
184 difference. In (Casper et al., 2016), they studied rear surface passivation of ultra-thin CIGS
185 solar cell, by using 25nm and 50nm thick Al_2O_3 as the passivation layer, and the contact
186 openings were realized by lithography, i.e., they had controlled size and distribution for the
187 openings. They experimentally proved that 90% surface coverage gave the best Voc. In
188 (Vermang et al., 2014a), on the other hand, it was mentioned that the 5% contact opening area,
189 i.e., 95% surface coverage, in 5nm thick Al_2O_3 layer is sufficient for passivation. In our case,
190 we got the best Voc from 6nm thick Al_2O_3 , i.e., 83% SC (Fig.3-a). The reason for this
191 difference can be explained by our novel approach. Since the size and the distribution of the
192 openings are reasonably random, and not yet controllable, it is reasonable to have slightly
193 different results from the literature. The detailed solar cell results will be shared and discussed
194 in the following section. The JV results showed that for 2nm (95% SC) and 4nm (90% SC)
195 thick layers, there was a little enhancement in Voc values as compared to the reference, i.e.,
196 unpassivated solar cell, but it was not as significant as a 6nm (83% SC) thick layer. Since the
197 effect of the rear surface passivation reveals itself as an increased diffusion length of the
198 minority carriers due to the created field effect, the difference in these results can be explained
199 by the insufficient thickness of the dielectric layer and the non-optimized contacting approach
200 (Kotipalli, 2016). For 8nm and 10nm thick layers, on the other hand, the current was almost
201 completely blocked, and the passivation layer acted as a barrier layer. The JV curves of those
202 samples showed us that the sample with an 8nm thick Al_2O_3 layer has suffered from low shunt
203 resistance, and the sample with a 10nm thick Al_2O_3 layer had high series resistance, both results
204 in low FF, hence low power conversion efficiency. (Supporting Figure 1) Therefore, we proved
205 that 8nm and 10nm are too thick for described alkali treatment to make sufficient openings
206 with our approach, and consequently, we decided to use a 6nm thick alumina layer for further
207 experiments.

208

209 *3.1.2 Effect of the molarity of the alkali solution, Set 2:*

210 After optimizing the thickness of the passivation layer to 6nm, we investigated the necessity of
211 the alkali treatment. To do so, two samples were prepared, one without any alkali treatment
212 and one with a 0.2M NaF solution. As can be seen from Figure-3-a, if we do not use any alkali
213 solution, there will be no opening-like structures in the alumina layer. On the other hand, for
214 the 0.2M NaF solution, we were able to detect and analyze the openings. There is a slight
215 difference in SC ratios between 0.2M (86.5% SC) and 0.4M (83% SC) NaF solutions.
216 However, if the solar cell parameters, especially the Voc, are compared, it is safe to say that
217 0.4M NaF works better than 0.2M NaF, see Figure-3-b.

218 According to the JV measurement, it is clear that the alkali treatment is necessary since the
219 current is completely blocked, resulting in diode like response under illumination, for the solar
220 cell that has no alkali treatment. Besides, for 0.4M NaF, as told earlier, we achieved better solar
221 cell characteristics in comparison to 0.2M NaF. The FF, for instance, is noticeably lower for
222 0.2M NaF sample, 20% less than 0.4M NaF sample, which was resulting in lower power
223 conversion efficiency. (Supporting Figure 2) This can be explained by the lack of contact
224 openings due to less alkali salt crystal and/or lack of Na supply due to low concentration.
225 Hence, we decided to use a 0.4M NaF solution from this point forward.

226

227 *3.1.3 Solar cells prepared with optimal conditions:*

228 After we validated our approach regarding the openings with the help of two sets of
229 characterization samples, the next step was to prove that our assumption is valid for finished
230 solar cells. We prepared a sample with the optimal conditions again. The first aim is to show
231 the process's repeatability, and the second aim is to use that sample for detailed electrical and
232 optical analysis. After completing the measurements, we picked the solar cell with the highest
233 efficiency, and then made a scratch with the help of a tweezer to remove the window layer and
234 the absorber layer. The aim is to prove that the contact openings are realized in the dielectric
235 layer during CIGS absorber layer deposition. Since we only mimicked the environment for
236 characterization samples, it is always possible that during the actual deposition, conditions can
237 slightly differ. After we made the scratch, we were able to prove that there were contact
238 openings created in the passivation layer for a finished solar cell as well, by using SEM and
239 EDS measurements. (Supporting Figure 3) As a result, we proved that with our novel approach,
240 contact openings could be realized in the dielectric passivation layer with a fast and cost-
241 effective technique.

242
243 **3.2 Electrical and optical analysis of the solar cell devices produced with optimal**
244 **parameters:**

245
246 In this section, we present the results of the solar simulator, EQE, and TRPL. The results of
247 these measurements will be shared and discussed in detail.

248 The arithmetic average of standard solar cell parameters for the 12 best cells for passivated and
249 reference samples is given in Table-3. Further, two passivated cells that have the best efficiency
250 and the best Voc when compared to the other cells are shared as well.

251 The addition of the passivation layer with contact openings leads to an increase in nearly all
252 solar cell parameters compared to standard unpassivated solar cells. We extracted the Jsc values
253 from the EQE for the best two solar cells only, in order to avoid potential errors caused by the
254 grids or scribing. Then, the power conversion efficiency values for those two best cells are
255 recalculated (Table-3). If we compare the Jsc value for the average passivated solar cells and
256 Jsc value that is extracted from the EQE for the best cells, we noticed a 5mA difference between
257 those values, see Table-3. The probable cause for this difference is explained in detail in
258 (Scheer and Schock, 2011).

259 As shared in Table-3, by the addition of a passivation layer with contact openings through an
260 easy and cost-effective way, we reached Voc of 623mV with ultra-thin single-stage CIGS solar
261 cells. If we examined even further, due to the 14% relative increase in open-circuit voltage,
262 i.e., from 536mV to 608mV, the power conversion efficiency of the passivated sample gained
263 a 24% relative increase, i.e., from 5.2% to 7.2%, for the average of twelve cells. Furthermore,
264 by using the extracted current values from EQE, i.e., corrected Jsc, we achieved 9.8% power
265 conversion efficiency.

266
267
268
269
270

271 **Table-3** JV parameter comparison between reference (bare) and passivated ultrathin CIGS
 272 solar cells. (average of 12 cells) Further, JV parameters of the cells that have the best efficiency
 273 and open-circuit voltage values for passivated solar cells. **Jsc values extracted from EQE and*
 274 *the power conversion efficiencies recalculated accordingly.*
 275

	Number of cells	Jsc (mA/cm ²)	Voc (mV)	FF (%)	Eta (%)
Reference- Average	12	20.9 ± 2.3	536 ± 28.1	51.8 ± 6.6	5.8 ± 1.1
Passivated- Average	12	19.9 ± 1.63	608 ± 8.9	59.6 ± 1.77	7.2 ± 0.7
Passivated- Best Eff.	1	25.1*	617.01	62.2	9.8*
Passivated- Best Voc	1	23.6*	622.84	56.9	8.4*

276
 277 The rear surface passivation effect can easily be explored by examining the differences between
 278 reference and passivated solar cells' Voc values. To this effect, the following simplified
 279 equation is used:

$$V_{oc} \approx \frac{k_B T}{q} \ln \left(\frac{J_{ph}}{J_0} \right) \quad \text{Eq.1}$$

282
 283 where J_{ph} is equal to short circuit current in an ideal case. Since the variation in J_{ph} is generally
 284 limited, the key element that determines the change in Voc is the saturation current density.
 285 The change in saturation current density (J_0) can be in orders of magnitudes, and this change
 286 depends on the recombination in the solar cell (Smets et al., 2016). Hence, lower J_0 means
 287 lower recombination, and eventually higher Voc. The addition of the aluminum oxide dielectric
 288 layer in combination with sodium fluoride decreases the J_0 noticeably, and causes a significant
 289 increase in Voc, see Table-4.

290 For further investigation, we update the Eq.1 to calculate the open-circuit voltage difference
 291 (ΔV_{oc}) between reference and passivated solar cells:

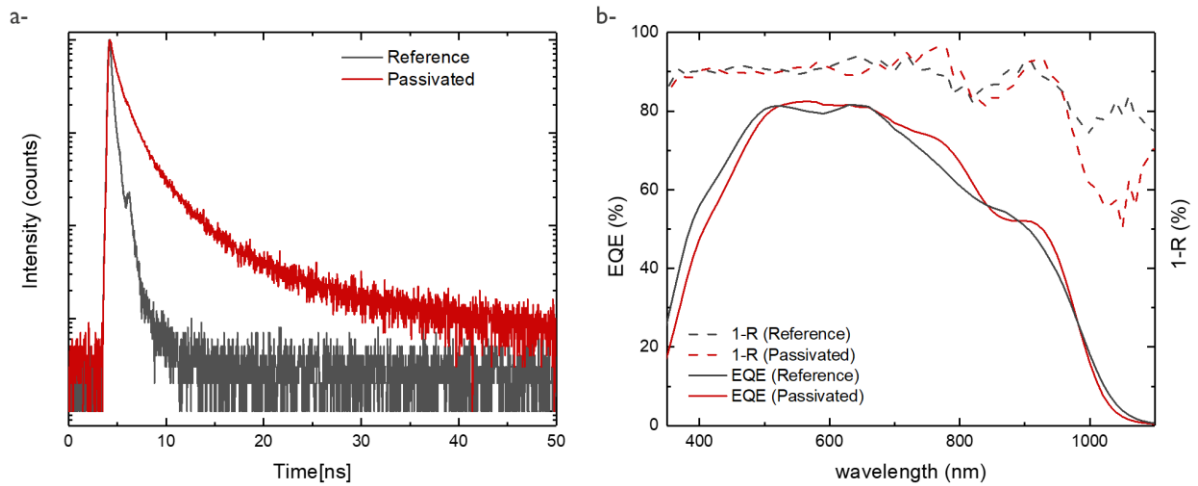
$$\Delta V_{oc} \approx \frac{k_B T}{q} \ln \left(\frac{J_{0,passivated}}{J_{0,reference}} \right) \quad \text{Eq.2}$$

294
 295 A random cell for reference and passivated sample, and the best efficient passivated solar cell
 296 are chosen and the measured J_0 and Voc values, ΔV_{oc} and calculated Voc values for those cells
 297 are given in Table-4.
 298
 299
 300
 301

302 **Table 4-** The saturated current density (J_0), measured open-circuit voltage (V_{oc-m}), the
 303 difference in Voc (ΔV_{oc}) (calculated from Eq.2) and the calculated open-circuit voltage (V_{oc-c})
 304 values are given for: the reference average, the passivated average, and the passivated-best
 305 efficient solar cells.

	J_0 (mA/cm ²)	V_{oc-m} (mV)	V_{oc-c} (mV)	ΔV_{oc}
Reference- average cell	$1.72E - 8$	562	-	-
Passivated-average cell	$5.63E - 9$	610	652.5	90.5
Passivated-best efficient cell	$5.62E - 10$	617.1	711.9	149.9

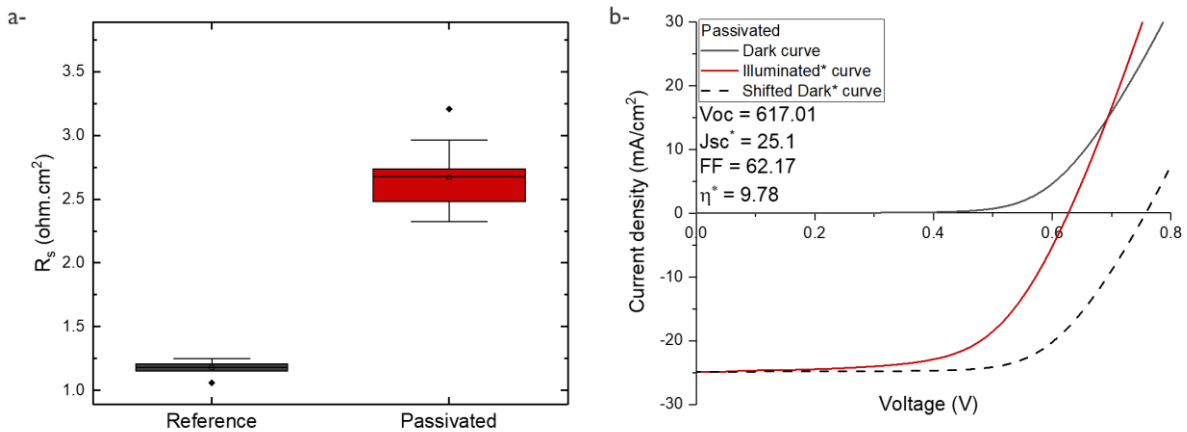
306
 307 According to the Table-4, the significant decrease in the J_0 results in an increase in Voc values.
 308 This increase implies that the reason for higher Voc is very likely due to reduced recombination
 309 at the rear surface. The reduced rear surface recombination should show itself clearly as an
 310 improved FF, as well (Vermang et al., 2014b), (Leilaeioun, 2018). However, our contacting
 311 approach is not optimized yet, so the increase in FF is somewhat limited. This limitation is due
 312 to the high series resistance (R_s) values for passivated solar cells. (Fig.5 a) The R_s values for
 313 passivated solar cells are significantly higher than the reference solar cells. This increase means
 314 that there is a lack of contact openings. Hence, our contacting approach needs further
 315 optimizations. In fact, after further optimizations, the calculated Voc values could be reached.
 316 If the TRPL and EQE results are investigated, it can be seen that the improvement in Voc is
 317 not related to optical enhancements, see Figure-4. The 1-Reflectance (1-R), is also given in
 318 Fig.4-b. Since the transmittance is nearly zero for our structure, 1-R can be accepted as the
 319 absorption of our solar cells. The TRPL measurement was performed on the finished solar
 320 cells. As can be seen from Fig.4-a, the passivated solar cell gave the slowest decay time. This
 321 slow decay arguably implies the reduced recombination at the rear surface. However, even for
 322 the passivated solar cell, the life-time is not at the same level as the state-of-the-art CIGS solar
 323 cells. At this point, one needs to remember that our absorber layer is ultra-thin (500nm) and
 324 non-graded. So, lower life-time values are expected.
 325



326
 327 **Figure 4** a-TRPL and b-smoothened EQE and 1-R of reference (black) and passivated (red)
 328 solar cells.

329
 330 For passivated solar cells, the EQE response is higher for long wavelengths. One known reason
 331 for this increase is the optical enhancement due to the contact openings. The bump around
 332 980nm for the passivated solar cell can be seen as an optical effect since a similar bump has
 333 been explained in detail for 390nm thick CIGS solar cells before, as an optical effect, see
 334 (Hegedus and Shafarman, 2004). On the other hand, the results coming from the reflectance
 335 measurement (1-R) for passivated and reference solar cells are quite similar. Hence, the
 336 increase in EQE can be associated with the rear-surface passivation effect rather than the optical
 337 enhancement.

338



339
 340 **Figure 5** a- Distribution of the series resistance values for reference (black) and passivated
 341 (red) solar cells and b- JV curve for the best efficient passivated solar cell with the shifted dark
 342 curve. * J_{sc} and efficiency values were extracted from EQE, and the associated curves also adapted for this
 343 change.

344

345 We also analyze the JV curve for the passivated sample to check if there are any anomalies,
 346 see Figure 5-b. Our JV curve seems to suffer from two anomalies: i-violation of superposition
 347 principle and ii-cross-over. In (Scheer and Schock, 2011), both of these anomalies and the
 348 reasons for them were discussed in detail. In our case, the most probable reasons for (i) is that

349 a- the boundary condition for quasi-neutral region (QNR) recombination is changed by large
350 series resistance, or b- due to light modulated potential barrier, the change from interface
351 recombination to Shockley Read Hall (SRH) recombination. We shifted the dark curve by J_{sc}
352 and compared it with the light curve. The aim is to see the V_{oc} without any light-induced defect
353 and/or recombination. (Fig. 5-b) Since the FF is increasing under light, the reason for this
354 anomaly, i.e., shifting violation, is most probably caused by high series resistance.
355 If we investigate the JV curve further, the second anomaly (ii) that we suffered from, the cross-
356 over phenomenon, can be seen (Igalson et al., 2009). Several possible reasons can cause this
357 anomaly, but the exact reason is still unknown. However, if we will be able to solve our high
358 series resistance problem, and by doing so, overcome the violation of shifting anomaly, we will
359 also be able to overcome the cross over phenomenon. If the shifted dark curve, i.e., the dashed
360 curve, is followed, it is clear that it will not cross the dark curve. (Fig. 5-b) Hence, reducing
361 the series resistance by optimizing our contacting approach will help us to overcome those
362 anomalies in the future. As a result, we can reach higher efficiencies.

363

364 **4. Conclusion and outlook:**

365 In summary, we fabricated ultrathin rear surface passivated solar cells with an industrially
366 viable, fast and novel process. The novelty of our process is to create the contact openings by
367 adding NaF solution by spin coating it on the alumina passivation layer. In this way, we
368 managed to detect the openings in the passivation layer by top-view SEM, even for the
369 complete solar cell. Even though we are still not able to thoroughly explain the origin of these
370 openings, it became clear that we need the alkali solution and the selenization at 540-degree
371 Celsius. After we were convinced that we managed to create the contact openings, we altered
372 the thickness of the passivation layer and the molarity of the alkali solution in pursuit of finding
373 the ultimate structure for best efficiency. As a result, we decided that 6nm alumina deposition
374 in combination with 0.4M NaF solution gives the best JV results. Hereby, we reached 623mV
375 V_{oc} , and for the best cell, we gained a 43% relative increase in power conversion efficiency.
376 The main advantage of this structure is that it is easy, fast and applicable to larger areas.
377 Considering that spin-coating is not an industrially feasible technique, instead of this, other
378 industrially feasible coating techniques, for example, slot dye technique, could be used for
379 sodium fluoride deposition. Even though this process is not as controllable as more standard
380 techniques, upon the repetition of our experiment, we obtained very similar results. So, it is
381 safe to say that the alterations, i.e. non-controllable elements, do not affect the efficiency
382 significantly. Moreover, it is possible to apply this structure to the front surface of CIGS solar
383 cells. The next step is to investigate further the chemistry and physics behind the creation of
384 the openings, and then optimize the process. After that, we believe that the calculated V_{oc}
385 values can be reached by reducing the series resistance.

386

387 **Acknowledgment:**

388 This work received funding from the European Unions H2020 research and innovation
389 program under grant agreement No. 715027.

390

391

392 **References:**

393 Birant, G., Wild, J. De, Meuris, M., Poortmans, J., Vermang, B., Pv, S., 2019. Dielectric-
394 Based Rear Surface Passivation Approaches for Cu (In , Ga) Se 2 Solar Cells — A
395 Review. *Appl. Sci.* 9. <https://doi.org/10.3390/app9040677>

396 Casper, P., Hünig, R., Gomard, G., Kiowski, O., Reitz, C., Lemmer, U., Powalla, M.,
397 Hetterich, M., 2016. Optoelectrical improvement of ultra-thin Cu (In,Ga)Se₂ solar cells
398 through microstructured MgF₂ and Al₂O₃ back contact passivation layer. *rrl Sol.* 376–
399 380. <https://doi.org/10.1002/pssr.201600018>

400 de Wild, J., Buldu, D.G., Schnabel, T., Simor, M., Kohl, T., Birant, G., Brammert, G.,
401 Meuris, M., Poortmans, J., Vermang, B., 2019. High Voc upon KF Post-Deposition
402 Treatment for Ultrathin Single-Stage Coevaporated Cu(In, Ga)Se₂ Solar Cells. *ACS*
403 *Appl. Energy Mater.* 2, 6102–6111. <https://doi.org/10.1021/acsaem.9b01370>

404 Green, M.A., Dunlop, E.D., Hohl-Ebinger, J., Yoshita, M., Kopidakis, N., Ho-Baillie,
405 A.W.Y., 2020. Solar cell efficiency tables (Version 55). *Prog. Photovoltaics Res. Appl.*
406 28, 3–15. <https://doi.org/10.1002/pip.3228>

407 Groner, M.D., Elam, J.W., Fabreguette, F.H., George, S.M., 2002. Electrical characterization
408 of thin Al₂O₃ films grown by atomic layer deposition on silicon and various metal
409 substrates. *Thin Solid Films* 413, 186–197.

410 Hegedus, S.S., Shafarman, W.N., 2004. Thin-film solar cells: device measurements and
411 analysis. *Prog. Photovoltaics Res. Appl.* 12, 155–176. <https://doi.org/10.1002/pip.518>

412 Igalson, M., Zabierowski, P., Prza, D., Urbaniak, A., Edoff, M., Shafarman, W.N., 2009.
413 Understanding defect-related issues limiting efficiency of CIGS solar cells. *Sol. Energy*
414 *Mater. Sol. Cells.* <https://doi.org/10.1016/j.solmat.2009.01.022>

415 Kotipalli, R.V.R., 2016. Surface Passivation Effects of Aluminum Oxide on Ultra-Thin CIGS
416 Solar Cells. Université Catholique de Louvain.

417 Ledinek, D., Donzel-gargand, O., Sköld, M., Keller, J., Edo, M., 2018. Effect of different Na
418 supply methods on thin Cu(In,Ga)Se₂ solar cells with Al₂O₃ rear passivation layers.
419 *Sol. Energy Mater. Sol. Cells* 187, 160–169.
420 <https://doi.org/10.1016/j.solmat.2018.07.017>

421 Leilaieoun, M., 2018. Fill Factor Loss Mechanisms: Analysis and Basic Understanding in
422 Silicon Hetero-junction Solar Cells. Arizona State University.

423 Li, W., Yan, X., Aberle, A.G., Venkataraj, S., 2019. Effect of sodium diffusion on the
424 properties of CIGS solar absorbers prepared using elemental Se in a two-step process.
425 *Sci. Rep.* 1–11. <https://doi.org/10.1038/s41598-019-39283-2>

426 Naghavi, N., Mollica, F., Goffard, J., Posada, J., Duchatelet, A., Jubault, M., Donsanti, F.,
427 Cattoni, A., Collin, S., Grand, P., Greffet, J., Lincot, D., 2016. Ultrathin Cu(In,Ga)Se₂
428 based solar cells. *Thin Solid Films.* <https://doi.org/10.1016/j.tsf.2016.11.029>

429 Necas, D., Klapetek, P., 2012. Gwyddion : an open-source software for SPM data analysis.
430 *Cent. Eur. J. Phys.* 10. <https://doi.org/10.2478/s11534-011-0096-2>

431 Poncelet, O., Kotipalli, R., Vermang, B., Macleod, A., Francis, L.A., Flandre, D., 2018.
432 Optimisation of rear reflectance in ultra-thin CIGS solar cells towards > 20 % efficiency.
433 *Sol. Energy Mater. Sol. Cells* 146, 443–452.
434 <https://doi.org/10.1016/j.solener.2017.03.001>

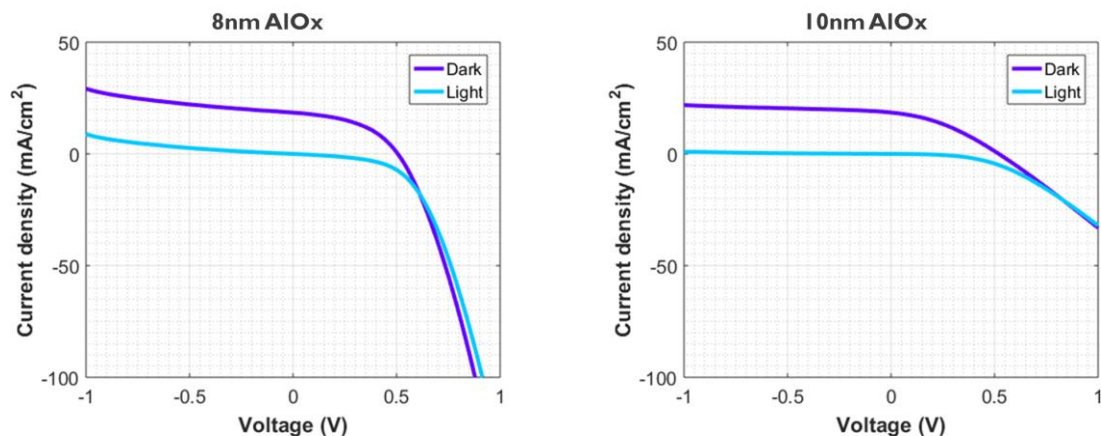
435 Poncelet, O., Kotipalli, R., Vermang, B., Macleod, A., Francis, L.A., Flandre, D., 2017.
436 Optimisation of rear reflectance in ultra-thin CIGS solar cells towards > 20 % efficiency.
437 *Sol. Energy* 146, 443–452. <https://doi.org/10.1016/j.solener.2017.03.001>

438 Rudmann, D., 2004. Effects of sodium on growth and properties of Cu(In,Ga)Se₂ thin films
439 and solar cells. Swiss Federal Institute of Technology (ETH) Zurich.
440 <https://doi.org/doi.org/10.3929/ethz-a-004796411>

441 Scheer, R., Schock, H., 2011. Chalcogenide Photovoltaics. WILEY-VCH.
442 <https://doi.org/10.1002/9783527633708>

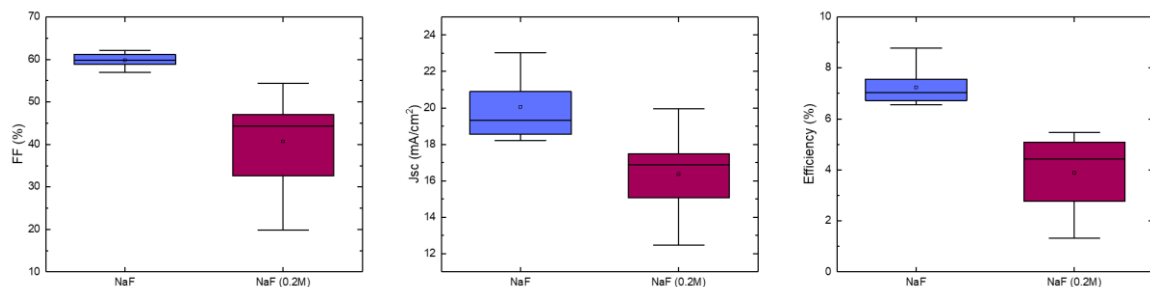
443 Smets, A.H.M., Jäger, K., Isabella, O., van Swaaij, R.A., Zeman, M., 2016. Solar Cell
 444 Parameters and Equivalent Circuit 9.1 External solar cell parameters. Sol. energy Phys.
 445 Eng. Photovolt. conversion, Technol. Syst. 113–121.
 446 Umehara, T., Iinuma, S., Yamada, A., 2016. Investigation of the effects of rear surface
 447 recombination on the Cu(In,Ga)Se₂ solar cell performances. Electron. Mater. Lett. 12,
 448 479–483. <https://doi.org/10.1007/s13391-016-4010-3>
 449 Vermang, B., Gao, X., Edoff, M., 2014a. Improved Rear Surface Passivation of
 450 Cu(In,Ga)Se₂ Solar Cells : A Combination of an Al₂O₃ Rear Surface Passivation Layer
 451 and Nanosized Local Rear Point Contacts 4, 486–492.
 452 <https://doi.org/10.1109/JPHOTOV.2013.2287769>
 453 Vermang, B., Timo, J., Fjällström, V., Rostvall, F., Edoff, M., Gunnarsson, R., Pilch, I.,
 454 Helmersson, U., Kotipalli, R., Henry, F., Flandre, D., 2015. Highly reflective rear
 455 surface passivation design for ultra-thin Cu(In,Ga)Se₂ solar cells. Thin Solid Films 582,
 456 300–303. <https://doi.org/10.1016/j.tsf.2014.10.050>
 457 Vermang, B., Wätjen, J.T., Fjällström, V., Rostvall, F., Edoff, M., Kotipalli, R., Henry, F.,
 458 Flandre, D., 2014b. Employing Si solar cell technology to increase efficiency of ultra-
 459 thin Cu(In,Ga)Se₂ solar cells. Prog. Photovoltaics Res. Appl. 22, 1023–1029.
 460 <https://doi.org/10.1002/pip.2527>
 461 Yin, G., Knight, M.W., Lare, M. Van, Magdalena, M., Garcia, S., Polman, A., Schmid, M.,
 462 2017. Optoelectronic Enhancement of Ultrathin CuIn_{1-x}Ga_xSe₂ Solar Cells by
 463 Nanophotonic Contacts. Adv. Opt. Mater. 5. <https://doi.org/10.1002/adom.201600637>
 464

465 **Supporting Information:**



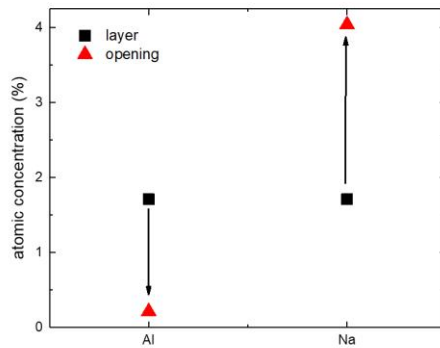
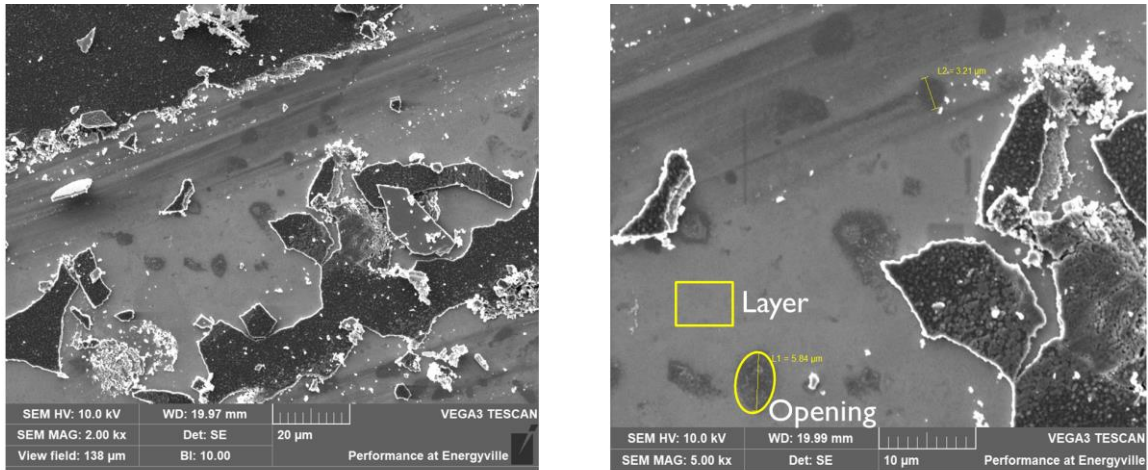
466
 467 Supported Figure 1 : IV curves for samples with 8nm and 10nm AlO_x layer.
 468

469



470
 471 Supported Figure 2 : Comparison of the solar cell parameters for the samples with 0.4M and
 472 0.2M NaF on top of 6nm AlO_x dielectric layer.

473
474



475
476
477
478
479
480
481
482
483

Supported Figure 3: EDS analysis and SEM pictures of openings from the complete cell structure. EDS measurement was done from layer and opening, and the atomic concentrations are shared as a graph to emphasize the change. The arrows indicate the direction of the change. As can be seen from the EDS graph, the Al signal drops nearly to zero, which means there is no Al signal through the opening. On the other hand, the Na signal increases from layer to openings. This indicates that aluminum oxide layer blocks the Na coming from the glass, and hence, from the openings, we observed higher Na signal.

Window and absorber layers removed via tweezers.